J Mater Sci (2009) 44:5318–5324
DOI 10.1007/s10853-009-3606-5

FERROELECTRICS

Effect of film thickness on ferroelectric domain structure and properties of $Pb(Zr_{0.35}Ti_{0.65})O_3/SrRuO_3/SrTiO_3$ heterostructures

Hitoshi Morioka · Keisuke Saito · Shintaro Yokoyama · Takahiro Oikawa · Toshiyuki Kurosawa · Hiroshi Funakubo

Received: 16 March 2009 / Accepted: 14 May 2009 / Published online: 30 May 2009

Abstract Epitaxial $Pb(Zr_{0.35}Ti_{0.65})O_3$ (PZT) thin films with tetragonal symmetry and thicknesses ranging from 45 to 230 nm were grown at 540 °C on $SrRuO_3$-coated (001)$SrTiO_3$ substrates by pulse-injected metalorganic chemical vapor deposition. The effect of the film thickness on the ferroelectric domain structure and the dielectric and ferroelectric properties were systematically investigated. Domain structure analysis of epitaxial PZT films was accomplished with high-resolution X-ray diffraction reciprocal space mapping and high-resolution transmission electron microscopy. Fully polar-axis (*c*-axis)-oriented epitaxial PZT thin films with high ferroelectric polarization values [e.g., remanent polarization (P_r) ~ 90 μC/cm^2] were observed for film thicknesses below 70 nm. Films thicker than 70 nm had a *c*/*a*/*c*/*a* polydomain structure and the relative volume fraction of *c*-domains monotonously decreased to about 72% on increasing the film thickness up to 230 nm , and finally P_r diminished to about 64 μC/cm^2 for the 230-nm-thick epitaxial film. These polarization values were in good agreement with the estimated values taking into account the volume fraction of the *c*-axis-oriented domains while assuming a negligible contribution of 90° domain reorientation caused by an externally applied electric field.

H. Morioka (✉) · K. Saito
Application Laboratory, Bruker AXS, 3-9-B-6F Moriya-cho Kanagawa-ku, Yokohama 221-0022, Japan
e-mail: hitoshi.morioka@bruker-axs.jp

T. Kurosawa
Bruker AXS, 3-9 Moriya-cho Kanagawa-ku, Yokohama 221-0022, Japan

H. Morioka · S. Yokoyama · T. Oikawa · H. Funakubo (✉)
Department of Innovative and Engineered Materials, Interdisciplinary Graduate School of Science and Engineering, Tokyo Institute of Technology, J2-15F, Mailbox J2-43, 4259 Nagatsuta-cho, Midori-ku, Yokohama 226-8502, Japan
e-mail: funakubo.h.aa@m.titech.ac.jp

Introduction

Lead- and/or bismuth-based ferroelectric materials are widely investigated not only academically but also industrially for use in nonvolatile ferroelectric random access memories (FeRAMs), micoroelectromechanical systems, and optical devices [1–5]. In particular, simple perovskite-type ferroelectric materials, such as $PbTiO_3$, $PbZrO_3$, $Pb(Zr,Ti)O_3$, $LiTaO_3$, and $BiFeO_3$, have superior and fascinating properties, for example, large remanent polarization (P_r), piezoelectric coefficient, electromechanical coupling coefficient, high translucency, and multiferroic properties [6–10]. Device designs exploiting these properties require an understanding of the fundamental properties of these functional materials. However, since it is still very hard to grow large enough single crystals of $Pb(Zr,Ti)O_3$ materials, their basic properties have to be estimated by reference to data on bulk ceramics, polycrystalline films, and epitaxial films. It is known that tetragonal $Pb(Zr,Ti)O_3$ has a *c*/*a*/*c*/*a* polydomain structure that arises from the relaxing of growth strain [11], and the effect of nonpolar *a*-domains on the ferroelectric properties has been investigated [12–14]. Previously, we reported on fully polar-axis (i.e., *c*-axis)-oriented epitaxial $Pb(Zr_{0.35}Ti_{0.65})O_3$ (PZT) film with a large saturation polarization (P_{sat}) [15], and investigated the Zr/(Zr + Ti) ratio dependency on P_{sat} [16].

In this study, we systematically grew epitaxial PZT films with thickness ranging from 45 to 230 nm on

$SrRuO_3$-coated (001)$SrTiO_3$ substrates by metalorganic chemical vapor deposition (MOCVD) and investigated the effects of film thickness on the ferroelectric domain structure and electrical properties in order to discuss in more detail our previous letter [15].

Experimental procedure

Sample preparation

Epitaxial PZT thin films with tetragonal symmetry and a Zr/(Zr + Ti) ratio of 0.35 were grown on $(001)_c SrRuO_3$//(001)$SrTiO_3$ substrates at a growth temperature (T_g) of 540 °C by pulse-injected MOCVD using an apparatus having a horizontal cold-wall reaction chamber. $Pb(C_{11}H_{19}O_2)_2$, $Zr(O \cdot t\text{-}C_4H_9)_4$, $Ti(O \cdot i\text{-}C_3H_7)_4$, and O_2 gas were used as sources for Pb, Zr, Ti, and oxidant, respectively [17]. Epitaxial $SrRuO_3$ films were pseudomorphically grown at 750 °C on (001)$SrTiO_3$ substrates by MOCVD from the $Sr(C_{11}H_{19}O_2)_2(C_8H_{23}N_5)_2$–$Ru(C_7H_{11})(C_7H_9)$ (Tosoh Corp.)–O_2 system [18, 19]. The pseudocubic Miller indices, which were designated by hkl_c, were used for $SrRuO_3$ in the present study. The $SrRuO_3$ films acted as not only bottom electrodes but also templates for the heteroepitaxial growth of PZT. The film thickness of PZT was varied from 45 to 230 nm by controlling the deposition time.

Characterization

The orientation of the deposited films was analyzed by the 2θ–ω scan with high-resolution X-ray diffraction (HRXRD) using a four-axis diffractometer and Cu $K\alpha_1$ radiation [20]. The $2\theta \times \omega$ space HRXRD reciprocal space mapping (HRXRD-RSM) was measured to estimate the out-of-plane and in-plane lattice parameters and the relative volume fraction of the *c*-domain ($V_c = V_{(001)}/[V_{(100)} + V_{(001)}]$) for the PZT films having a mixture orientation of (001) (*c*-domain) and (100) (*a*-domain) [14]. The microstructures of the films and the interfaces between the PZT films and the bottom electrodes were characterized with cross-sectional transmission electron microscopy (TEM, JEOL JEM-3010). Samples for the TEM observation were prepared with a focused ion-beam-milling technique (FIB, Hitachi FB2100).

The electrical properties of the films were characterized with Pt/PZT/$SrRuO_3$ capacitors by making vacuum-evaporated Pt top electrodes through a 100 μm ∅ shadow mask. The top electrode area was measured with an optical microscope. The polarization–electric field (*P*–*E*) hysteresis loops of the as-deposited films were measured using pulsed rectangular waves (Radiant Technologies RT6000HVS and TOYO Corporation FCE-1). Saturation properties of the hysteresis loops were measured by decreasing the applied electric field from the maximum electric field. The P_{sat} is given by the *y* intercept of the tangent to the maximum polarization to the *P*–*E* hysteresis loops. The dielectric constant and leakage current density were measured using an impedance analyzer (HP 4194A) and a semiconductor parameter analyzer (Agilent 4155B), respectively.

Results and discussion

Crystal structure

Figure 1a–c shows the results of the HRXRD 2θ–ω scans measured around 002/200 PZT for 50-, 150-, and 230-nm-thick PZT films, respectively. The so-called cube-on-cube epitaxial relationships of these heterostructures were ascertained for (001)(100)[100][001]PZT//$(001)_c[100]_c SrRuO_3$//(001)[100]$SrTiO_3$ by performing an X-ray pole figure measurement at the fixed 2θ angle corresponding to the 111 PZT diffraction [17]. These results show that the 150- and 230-nm-thick PZT films consisted of mixed *a*- and *c*-domains, whereas the 50-nm-thick PZT films appeared to be only *c*-domain. The full width at half maximum (FWHM) values of the X-ray rocking curves for 004 PZT diffraction were 0.34° and 0.96° for the 50- and 230-nm-thick films, respectively, suggesting that the 50-nm-thick film had lower mosaicity in its crystallographic tilt compared with the 230-nm-thick film, because it does not exhibit the 90° domain structure. Note that the FWHM values of 004 $SrTiO_3$ and 004 $SrRuO_3$ were about 0.05° and 0.07°, respectively. The HRXRD-RSM results apparently demonstrate the changing domain structure from single *c*-domain to *c*/*a*/*c*/*a* polydomain subject on increasing the PZT film thickness

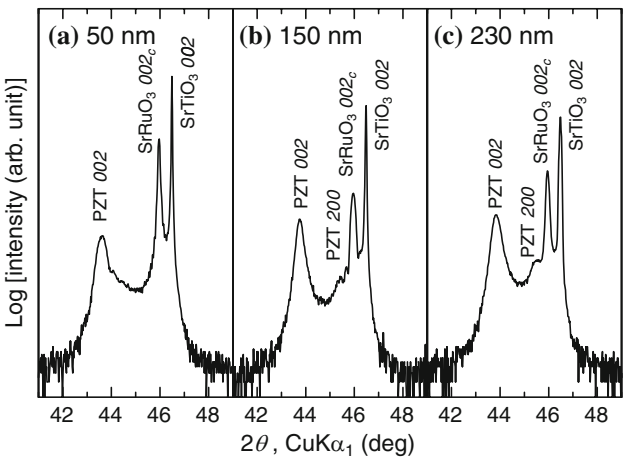

Fig. 1 High-resolution X-ray diffraction 2θ–ω scan patterns for **a** 50-, **b** 150-, and **c** 230-nm-thick PZT films measured around 002/200 PZT

[14, 15]. These results clearly show that the 50-nm-thick PZT film had only polar-axis-oriented domains with higher crystallographic completeness compared to thicker films induced by film thickness effect.

Figure 2a shows the relationship between PZT film thickness and V_c as estimated from the HRXRD-RSM analysis of the epitaxial PZT films. PZT films with thicknesses less than 70 nm had a fully polar-axis-oriented domain structure, and V_c monotonously decreased with increasing PZT film thickness up to 230 nm. The decrease followed the trend of the previously reported data [21, 22]. Figure 2b, c shows the relationship between PZT film thickness, the lattice parameters, and their *c*/*a* ratio of PZT films obtained from the HRXRD-RSM results, including the in-plane *a*-axis ($a_{//}$) and out-of-plane *c*-axis ($c_{\perp}$) of *c*-domain and the in-plane *c*-axis ($c_{//}$) and out-of-plane *a*-axis ($a_{\perp}$) of *a*-domain. The lattice parameter of substrate $SrTiO_3$ (=0.3905 nm) and unstrained state PZT with same Zr/(Zr + Ti) composition ($a = 0.398$ nm and $c = 0.413$ nm [23]) are also shown in Fig. 2b. The lattice parameters and *c*/*a* ratios of PZT films were almost constant for the whole range of PZT film thicknesses in the present study, and they demonstrated the fully relaxed unit cells that were different from those of fully strained pseudomorphic crystal growth in compound semiconductors, such as Si/SiGe [24]. This is due to the larger lattice mismatch between PZT films and $SrTiO_3$ substrates.

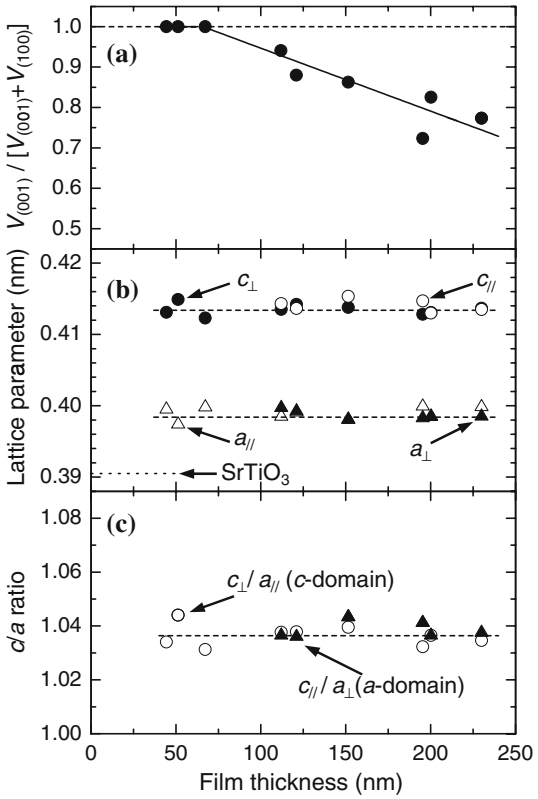

Fig. 2 Thickness dependence of **a** volume fraction of the *c*-domain (V_c) for PZT, **b** lattice parameters, and **c** the *c*/*a* ratio estimated from HRXRD-RSM results for epitaxial PZT films. Triangles (*filled triangle*, *open triangle*) and circles (*filled circle*, *open circle*) in (**b**) indicate the *a*- and *c*-axis, respectively, of tetragonal PZT. Filled and open symbols indicate out-of-plane and in-plane, respectively. The lattice parameter of the substrate ($SrTiO_3 = 0.3905$ nm) and unstrained state PZT powder with same Zr/(Zr + Ti) ratio ($a = 0.398$ nm and $c = 0.413$ nm [23]) are also shown in (**b**). The filled triangles and open circles in (**c**) indicate the *c*/*a* ratio for *a*- and *c*-domain, respectively, of PZT

As is well known, the ferroelectric materials show the strain dependence of their various properties, e.g., the domain structure, phase transition temperature, dielectric property, and piezoelectric property [25]. Thus, the strain effect was estimated from the observation of Curie temperature (T_C) shift by the high-temperature XRD 2θ–ω measurement around the 004 PZT and 004 $SrTiO_3$ at atmospheric conditions, because T_C is noted to be extremely sensitive to the strain. Figure 3 shows the trend of the out-of-plane *c*-axis lattice parameter for 50-nm-thick PZT film and substrate $SrTiO_3$ for the temperature ranging from room temperature to 600 °C over the growth temperature. Obvious discontinuous behavior of *c*-axis lattice parameter of PZT originated in the phase transition from tetragonal [*P*4*mm*] to cubic [$Pm\bar{3}m$] was observed at approximately 450 °C, and this temperature is well within the range of reported values for powder with same Zr/(Zr + Ti) composition [7]. This result also indicates the small residual strain in the fully polar-axis-oriented 50-nm-thick PZT films.

The relationships between the kind of cubic substrates and the V_c for not only PZT but also $PbTiO_3$ have been theoretically and experimentally investigated by many research groups including us [11, 21, 26–32]. The elastic strain is due to the mismatches in the lattice parameters and the thermal expansion coefficients of the substrate and PZT films introduced into the film lattice at growth and cooling

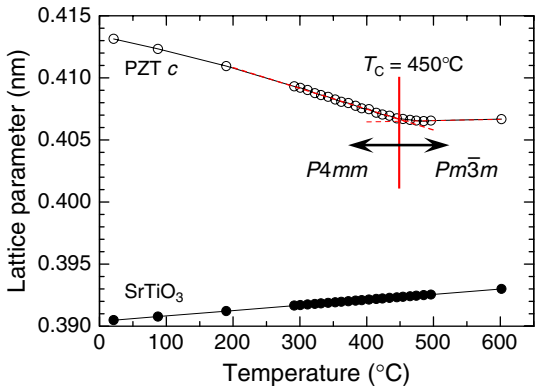

Fig. 3 The relationship between temperature and the lattice parameters of $SrTiO_3$ substrate and *c*-axis of PZT film for 50-nm-thick epitaxial PZT with single polar-axis-orientation

process, and these strains will be released by the generation of misfit dislocations and phase transition at T_C. This elastic-strain status can be described by the summation of the effective misfit strain (ε_m) [11] at T_g and the thermal strain (ε_{th}) stored in the cubic phase. Using an effective substrate lattice parameter, $b^*(T) = b(T_g)(1 - \rho_{md}|\mathbf{b}|\cos\lambda)$, which indicates the PZT thickness dependence, the effective misfit strain can be described as $\varepsilon_m^* = (b^* - a_c)/b^*$, where ρ_{md} is the dislocation density, **b** is the Burgers vector, and a_c is the lattice parameter of cubic phase PZT. Now, we considered the $\{101\}\langle 10\bar{1}\rangle$ slip system common for a cubic perovskite [11] and calculated the equilibrium dislocation density, ρ_{md}, based on the Matthews–Blakeslee criteria [33]. The thermal strain applied to the cubic PZT is described by $\varepsilon_{th} = (\alpha_{film} - \alpha_{sub})(T_g - T_C)$, where α_{film} and α_{sub} are the thermal expansion coefficients of the PZT film and $SrTiO_3$ substrate, respectively. The calculated total elastic-strain of $(\varepsilon_m^* + \varepsilon_{th})$ was about −0.001 (compressive) for the PZT/$SrRuO_3$/$SrTiO_3$ heterostructure system with thicknesses less than 70 nm. This calculated value is in close agreement with the $PbTiO_3$/(001)$SrTiO_3$ system with a 100% *c*-domain structure [26]. On the other hand, $(\varepsilon_m^* + \varepsilon_{th})$ shows the PZT thickness dependence and asymptotically approaches to 0 with increasing PZT thickness. Therefore, the PZT films show a fully polar-axis-orientation for thicknesses below 70 nm and the V_c decreases with increasing film thickness.

Figure 4a, b shows a cross-sectional TEM image and a selected-area diffraction pattern (SADP) of the 50-nm-thick epitaxial PZT film with full polar-axis-orientation. This TEM image shows that the interface between the PZT and $SrRuO_3$ bottom electrode was smooth and atomically sharp. In addition, no characteristic 90° domain stripe microstructure was observed unlike that observed in previous reports [21, 26, 34]. The SADP also shows that PZT crystal lattice was fully relaxed because the difference between in-plane lattice parameters for PZT and $SrRuO_3$ was the same as that given by the results of HRXRD-RSM. Therefore, the observed electrical properties, which are discussed in the next section, were fundamental data for PZT without large lattice strain effects characterized by the XRD and TEM analyses.

Electrical properties

Figure 5 plots the relative dielectric constant (ε_r) measured at room temperature and 1 kHz frequency with 20 mV amplitude voltage as a function of the film thickness for epitaxial PZT films. The ε_r had a smaller thickness dependence than that previously reported [35, 36]. This limited thickness dependence is what one would expect if there was a relatively small difference in the relative dielectric constant of the *a*- and *c*-domains, because of $\varepsilon_r \sim 500$ for $V_c \sim 0.05$ and $\varepsilon_r \sim 300$ for $V_c \sim 1.0$ [32], the small V_c change with film thickness in Fig. 5 [$V_c = 0.7$–1.0], and no substantial intermediate layer between epitaxial PZT and $SrRuO_3$ films (see Fig. 4).

Figure 6a, b shows *P*–*E* hysteresis loops measured at 20 Hz for epitaxial PZT films having 50 nm thickness ($V_c = 1.0$) and 230 nm thickness ($V_c = 0.72$), and Fig. 6c shows the saturation properties of the remanent polarization (P_r) and coercive field (E_c) versus the applied voltage for the same 50- and 230-nm-thick PZT films whose results are depicted in Fig. 6a, b. Well-saturated hysteresis loops with good squareness were observed for both epitaxial PZT films regardless of the difference in V_c and film thickness. In addition, a larger P_r value was observed for the 50-nm-thick films with large V_c. The 50-nm-thick PZT film also had a low voltage saturation of about 1.0 V (Fig. 6c). This well-defined hysteresis loop and P_r value of fully polar-axis-oriented PZT film were fairly close to values reported for 90° domain rotated $Pb(Zr_{0.2}Ti_{0.8})O_3$ island [12], defect-free single-crystalline $Pb(Zr_{0.2}Ti_{0.8})O_3$ film [37], and low-dislocation-density $Pb(Zr_{0.2}Ti_{0.8})O_3$ film [38] by other research groups.

Figure 7a–d plots P_{sat}, P_r, the ratio of P_r to P_{sat} (P_r/P_{sat}), and the normalized polarization P_N as a function of film

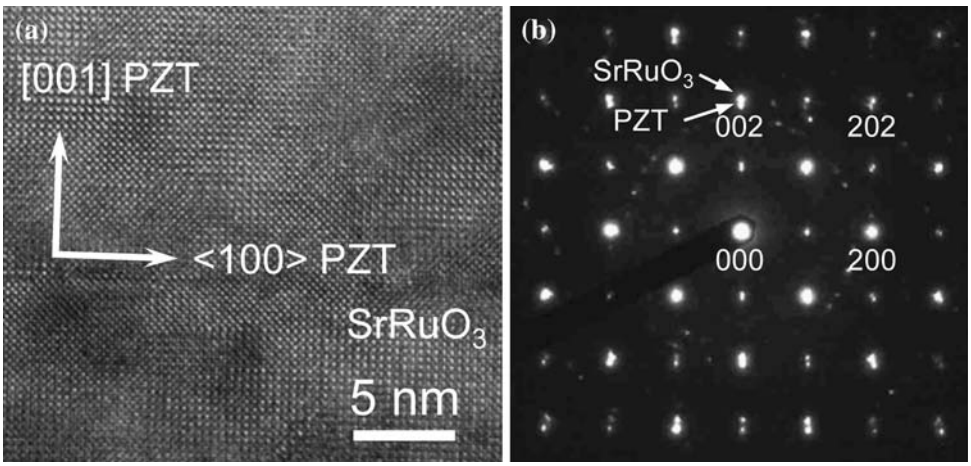

Fig. 4 **a** Cross-sectional high-resolution transmission electron microscopy image projected to ⟨100⟩ PZT of the PZT/$SrRuO_3$/$SrTiO_3$ heterostructure and **b** the selected-area diffraction pattern of the interface between PZT and $SrRuO_3$ for 50-nm-thick PZT film

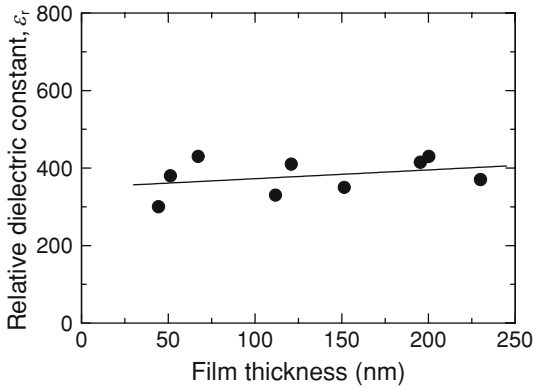

Fig. 5 Thickness dependence of the relative dielectric constant (ε_r) for epitaxial PZT thin films measured at room temperature and 1 kHz frequency with 20 mV amplitude voltage

thickness for epitaxial PZT heterostructures. The normalized polarization P_N is defined as P_r/V_c to elucidate the contribution of the *a*-domain to the polarization, based on the assumption that the ferroelastic *a*-domain did not reorient under an externally applied electric field. The P_{sat} and P_r had thickness dependences similar to those of V_c in Fig. 2a. These results show that the ferroelectric polarization strongly depends on the volume fraction of polar-axis-oriented domain and their polarization vectors [14, 39, 40]. The P_r/P_{sat} ratios, which indicate the squareness of *P–E* hysteresis loops, were almost constant above 0.9 for all films in this study, because of the similar square shape in *P–E* hysteresis loops for 50- and 230-nm-thick PZT films as demonstrated in Fig. 6 and similar tendencies of P_r and P_{sat} in Fig. 7a, b. Moreover, the P_N values are about 90 ± 10 μC/cm^2 regardless of the PZT thickness range from 45 to 230 nm. This result suggested that the reduction of the polarization on increasing the PZT film thickness was explained by the decrease in the V_c as shown in Fig. 2a. Here, we consider the role of in-plane stresses affecting the out-of-plane polarization. In the case of epitaxial $BaTiO_3$ thin films, there was a clearly observed enhancement in $T_C \sim 680$ °C and $P_r \sim 70$ μC/cm^2 which are about 5.2 and 2.7 times, respectively, higher than those of bulk single crystal in (001)$BaTiO_3$/(001)$_c$$SrRuO_3$/(001)$_c$$DyScO_3$ heterostructure with in-plane compressive strain [41]. This result is a typical example of the in-plane stress effect on ferroelectric properties along the out-of-plane direction. In contrast, the present PZT films were almost fully relaxed because the observed T_C was similar to that reported for powder (see Fig. 3) and the lattice parameters and *c*/*a* ratios did not change with decreasing thickness as mentioned above (see Fig. 2b). In addition, Lee et al. pointed out that $PbTiO_3$ and PZT are rather

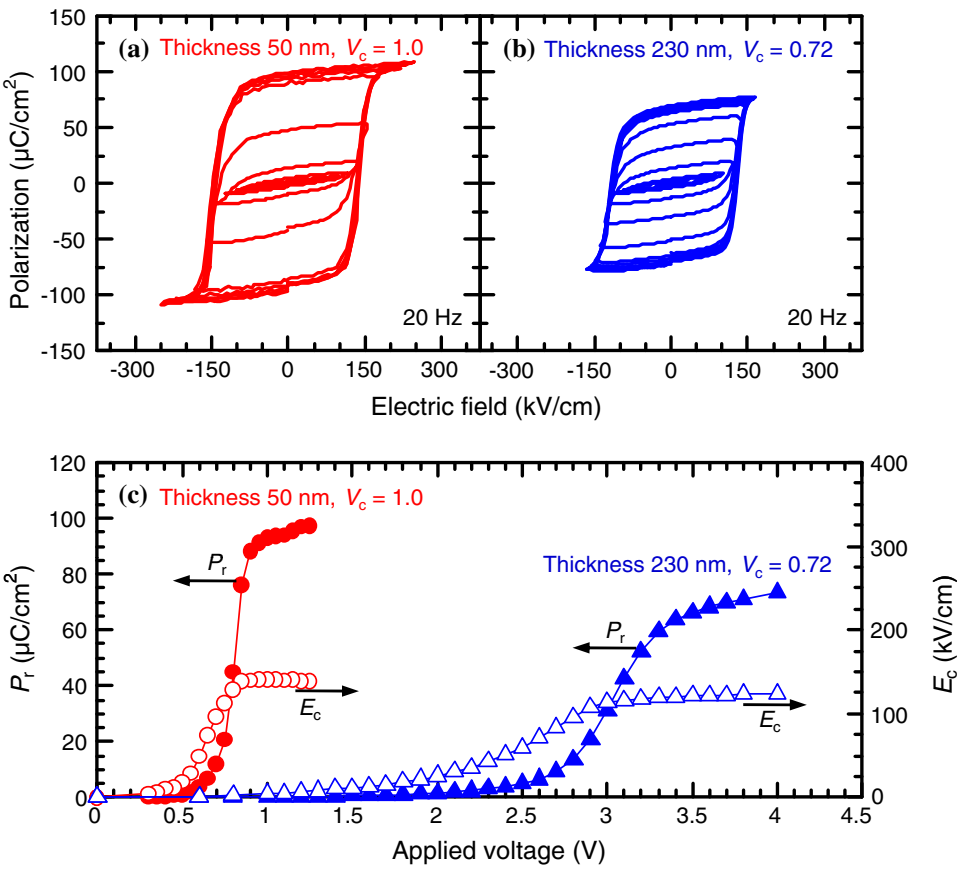

Fig. 6 **a** and **b** *P–E* hysteresis loops of 50- and 230-nm-thick PZT films and **c** saturation property of P_r and E_c against the maximum applied voltage as measured with a 20 Hz rectangular wave for the Pt/PZT/$SrRuO_3$/$SrTiO_3$ heterostructure

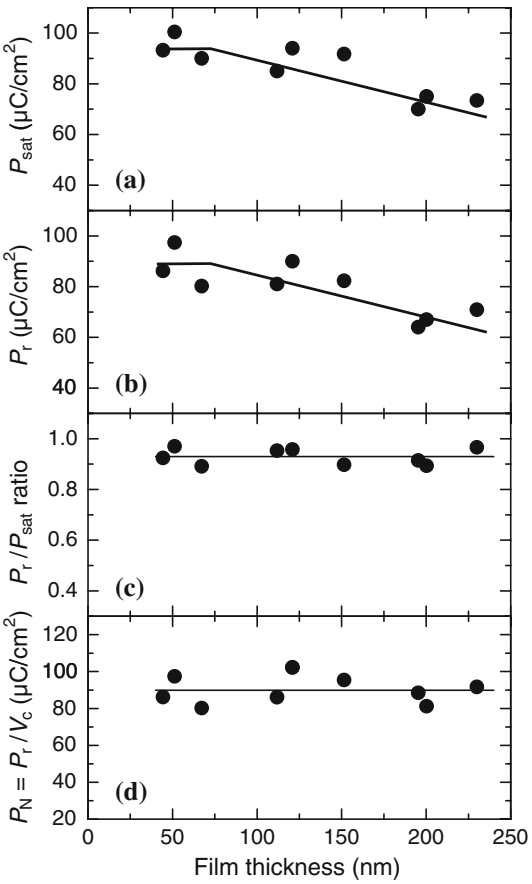

Fig. 7 **a** P_{sat}, **b** P_r, **c** the P_r/P_{sat} ratio, and **d** normalized polarization P_N as functions of PZT film thickness. The normalized polarization P_N is defined as P_r/V_c

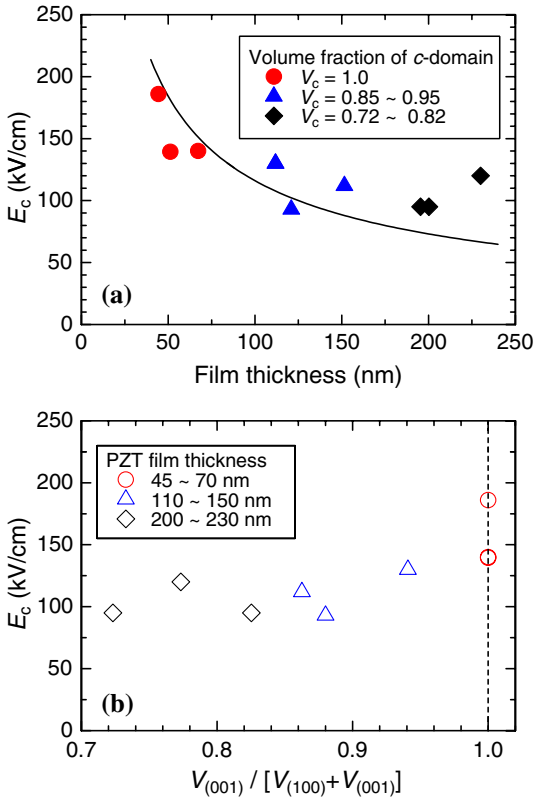

Fig. 8 Dependence of E_c on **a** PZT film thickness and **b** volume fraction of the *c*-domain, V_c. Closed symbols (*filled circle*, *filled triangle*, and *filled diamond*) indicate $V_c = 1.0$, 0.85–0.95, and 0.72–0.82. The scaling behavior curve [$E_c(d) \propto d^{-2/3}$] is shown as a solid line to guide the eye in (**a**). Open symbols (*open circle*, *open triangle*, and *open diamond*) in (**b**) indicate PZT film thickness of 45–70, 110–150, and 200–230 nm

insensitive than $BaTiO_3$ to applied external stress from a view point of the ferroelectric ionic displacements, especially *A*-site cations and equatorial oxygens [38]. Based on the reasons mentioned above, the stress-induced modification of ferroelectric properties can be almost neglected. Furthermore, the P_N values were well accorded with the previously estimated values of 87 μC/cm^2 [14, 40] and the calculated value of 85 μC/cm^2 from the Berry phase based on the first-principles calculation by Miyazawa (private communication). These results suggest that the observed ferroelectric polarization almost independent of the PZT film thickness are well explained by taking into account the V_c assuming that the 90° domain was not reoriented by an externally applied electric field in the PZT films.

Figure 8a, b shows the E_c as a function of PZT film thickness and V_c, respectively. The E_c follows the Kay and Dunn scaling law [$E_c(d) \propto d^{-2/3}$] (a guide to the eye in Fig. 8a) [42] for the whole film thickness range in this study (45–230 nm), in good agreement with various previous reports [43–46], and is undisturbed by the change of V_c determined by PZT film thickness as shown in Fig. 2a. Therefore, these results indicate that the E_c for the device can be controlled by taking account of the film thickness and composition dependence of E_c which is widely reported elsewhere [7, 47, 48].

Conclusions

Epitaxial PZT films ranging in thickness from 45 to 230 nm were grown on $SrRuO_3$-coated (001)$SrTiO_3$ substrates at 540 °C by pulse-injected MOCVD, and the effects of the film thickness on the domain structure and electrical properties were investigated. By characterizing the V_c by HRXRD-RSM measurement, the films with thickness less than 70 nm were found to have a fully polar-axis-orientated domain structure. The 50-nm-thick PZT films with full polar-axis orientation had larger P_r and P_{sat} than those of the *a*-/*c*-domain coexistent ones and a low voltage saturation property at an applied voltage of 1.0 V. The E_c depended on PZT film thickness according to a scaling law that was almost independent of V_c. However, ε_r and the P_r/P_{sat} ratio did not strongly depend on the film

thickness. These results indicate that the (001)/(100)-oriented tetragonal PZT films have favorable *P–E* hysteresis loop squareness with a large P_s, and these results may have applications to low voltage FeRAM if the substrate induced stress effects can be controlled when PZT film is grown on Si wafers.

Acknowledgements This research was carried out under the auspices of a Grant-in-Aid for Science Research on Priority Area (B) "Control of Material Property of Ferroelectric Thin Films and Their Application to a Next-Generation Memory Device." One of the authors (HM) would like to thank H. Miyazawa, Seiko-Epson Ltd., for useful advice on the theoretical calculation of the remanent polarization of PZT, M. Tanaka and Y. Miyamoto for TEM observations and fruitful discussions, and Prof. J. S. Cross, Tokyo Institute of Technology, for fruitful discussions.

References

1. Waser R (2003) Nanoelectrics and information technology. Wiley-VCH, Weinheim
2. Setter N, Damjanovic D, Eng L, Fox G, Gevorgian S, Hong S, Kingon A, Kohlstedt H, Park NY, Stepenson GB, Stolitchnov I, Taganstev AK, Taylor DV, Yamada T, Streiffer S (2006) J Appl Phys 100:051606
3. Auciello O, Scott JF, Ramesh R (1998) Phys Today 51:22
4. Lee HN, Hesse D, Zakharov N, Gösele U (2002) Science 296: 2006
5. Sato K, Kondo M, Kurihara K (2007) J Appl Phys 102:054104
6. Foster CM, Bai GR, Csencsits R, Vetrone J, Jammy R, Wills LA, Carr E, Amano J (1997) J Appl Phys 81:2349
7. Jaffe B, Cook W, Jaffe H (1971) Piezoelectric ceramics. Academic Press, London
8. Heartiling GH, Land CE (1971) J Am Ceram Soc 54:1
9. Bruner A, Eger D, Oron MB, Blau P, Katz M, Ruschin S (2003) Opt Lett 28:194
10. Wang J, Neaton JB, Zheng H, Nagarajan V, Ogale SB, Liu B, Viehland D, Vaithyanathan V, Schlom DG, Waghmare UV, Spaldin NA, Rabe KM, Wuttig M, Ramesh R (2003) Science 299:1719
11. Speck JS, Pompe W (1994) J Appl Phys 76:466
12. Nagarajan V, Roytburd A, Stanishevsky A, Prasertchoung S, Zhao T, Chen L, Melngailis J, Auciello O, Ramesh R (2003) Nat Mater 2:43
13. Tsurumi T, Kumano Y, Ohashi N, Takenaka T, Fukunaga O (1997) Jpn J Appl Phys 36:5970
14. Saito K, Kurosawa T, Akai T, Oikawa T, Funakubo H (2003) J Appl Phys 93:545
15. Morioka H, Asano G, Oikawa T, Funakubo H, Saito K (2003) Appl Phys Lett 82:4761
16. Morioka H, Yokoyama S, Oikawa T, Funakubo H, Saito K (2004) Appl Phys Lett 85:3516
17. Nagashima K, Aratani M, Funakubo H (2001) J Appl Phys 89:4517
18. Okuda N, Saito K, Funakubo H (2000) Jpn J Appl Phys 39:572
19. Higashi N, Watanabe T, Saito K, Yamaji I, Akai T, Funakubo H (2001) J Cryst Growth 229:450
20. Saito K, Kurosawa T, Akai T, Yokoyama S, Morioka H, Funakubo H (2005) In: Waser R, Böttger U, Tiedke S (eds) Polar oxides: properties, characterization, and imaging. Wiley-VCH, Weinheim
21. Nagarajan V, Jenkins IG, Alpay SP, Li H, Aggarwal S, Salamanca-Riba L, Roytburd AL, Ramesh R (1999) J Appl Phys 86:595
22. Kim YK, Lee K, Baik S (1999) J Appl Phys 95:236
23. Shirane G, Suzuki K (1952) J Phys Soc Jpn 7:333
24. Usami N, Nose Y, Fujiwara K, Nakajima K (2006) Appl Phys Lett 88:221912
25. Koukhar VG, Pertsev NA, Waser R (2001) Phys Rev B 64: 214103
26. Lee KS, Choi JH, Lee JY, Baik S (2001) J Appl Phys 90:4095
27. Hsu WY, Raj R (1995) Appl Phys Lett 67:729
28. Foster CM, Pompe W, Daykin AC, Speck JS (1996) J Appl Phys 79:1405
29. Roytburd AL (1998) J Appl Phys 83:228
30. Roytburd AL (1998) J Appl Phys 83:239
31. Alpay SP, Roytburd AL (1998) J Appl Phys 83:4714
32. Kim YK, Morioka H, Ueno R, Yokoyama S, Funakubo H (2005) Appl Phys Lett 86:212905
33. Matthews JW, Blakeslee AE (1974) J Cryst Growth 27:118
34. Kiguchi T, Wakiya N, Shinozaki K, Mizutani N (2003) Microelectr Eng 66:708
35. Amanuma K, Mori T, Hase T, Sakuma T, Ochi A, Miyasaka Y (1993) Jpn J Appl Phys 32:4150
36. Tokita K, Aratani M, Ozeki T, Funakubo H (2002) Key Eng Mater 216:83
37. Vrejoiu I, Rhun GL, Pintilie L, Hesse D, Alexe M, Gösele U (2006) Adv Mater 18:1657
38. Lee HN, Nakhmanson SM, Chisholm MF, Christen HM, Rabe KM, Vanderbilt D (2007) Phys Rev Lett 98:217602
39. Kiguchi T, Wakiya N, Shinozaki K, Mizutani N (2003) Mater Res Soc Symp Proc 748:U5.1
40. Funakubo H, Aratani M, Oikawa T, Tokita K, Saito K (2002) J Appl Phys 92:6768
41. Choi KJ, Biegalski M, Li YL, Sharan A, Shubert J, Uecker R, Reiche P, Chen YB, Pan XQ, Gopalan V, Chen L-Qm, Schlom DG, Eom CB (2004) Science 306:1005
42. Hay HF, Dunn JW (1962) Philos Mag 7:2027
43. Fujisawa H, Nakashima S, Kaibara K, Shimizu M, Niu H (1999) Jpn J Appl Phys 38:5392
44. Lin CH, Friddle PA, Ma CH, Daga A, Chen H (2001) J Appl Phys 90:1509
45. Pertsev NA, Contreras JR, Kukhar VG, Hermanns B, Kohlstedt H, Waser R (2003) Appl Phys Lett 83:3356
46. Scott JF (2006) J Phys: Condens Matter 18:361
47. Kim DJ, Maria JP, Kingon AI, Streiffer SK (2003) J Appl Phys 93:5568
48. Oikawa T, Aratani M, Funakubo H, Saito K, Mizuhira M (2004) J Appl Phys 95:3111